

Vulnerability analysis method of vegetation due to groundwater table drawdown induced by tunnel drainage

Cagri Gokdemir^a, Yoram Rubin^b, Xiaojun Li^{a,*}, Yandong Li^a, Hao Xu^a

^a Department of Geotechnical Engineering, College of Civil Engineering, Tongji University, 1239 Siping Road, Shanghai 200092, China

^b Department of Civil and Environmental Engineering, University of California, Berkeley, CA 94720-1716, United States

ARTICLE INFO

Keywords:

Unsaturated flow
Environmental impacts
Tunnel discharge
Critical zone

ABSTRACT

Tunnel drainage demonstrates a behavior that constantly drains the high-ground subsurface water that feeds the overlying vegetative cover. The environmental impact of construction process on groundwater table drawdown can be evaluated using groundwater models. However, considering only the effects of drawdown is insufficient to evaluate the vulnerability between the terrain surface and groundwater table. We proposed a vulnerability analysis method based on soil water pressure by including the Soil-Plant-Atmosphere Continuum (SPAC) approach. We defined the vulnerability based on the wilting point of the terrain vegetation. A theoretical case study representing the groundwater level alterations that induce permanent wilting was investigated. The vulnerability analysis method takes account of two important factors; vegetation type and soil textures. The results show that wilting is more infiltration dependent, therefore, it does not occur immediately once the water table is lower than rooting depth. Soil water pressure losses caused by groundwater table drawdowns are compensated when sufficient infiltration occurs. Without sufficient infiltration, soil texture is an important factor for the resilience of vegetation cover under the influence of groundwater table drawdown. In our case study, layered soils lead to a flow behavior which makes the vegetation reach permanent wilting earlier than the homogeneous counterpart. Vulnerability analysis of vegetation cover can be regarded as an important step for an environment-friendly tunnel drainage design.

1. Introduction

Deep underground discharge caused by tunneling systems may lead to fundamental changes in the flow dynamics of both saturated (Scheidler et al., 2017) and vadose zones (Kong et al., 2015). The impact of underground tunnel discharge has received little attention from eco-hydrological perspective despite of having observable effects on groundwater and surface water (Butscher et al., 2011; Chiu and Chia, 2012; Kim and Lee, 2008; Kværner and Snilsberg, 2008; Li et al., 2016a). Hydrological, hydrogeological, and environmental impacts on local ecosystem resulting from drawdown induced by tunnel excavation is attracting more research attention (Cesano et al., 2000; Raposo et al., 2010; Sweetenham et al., 2017; Vincenzi et al., 2009, 2014; Wang et al., 2017). Groundwater inflow during excavation may cause large drawdowns in the groundwater table, thus affecting the energy-water balance of any associated ecosystems, as reported in a study of a high-speed railway tunneling between Malaga and Cordoba, Spain (Gisbert et al., 2009). Most inter-city underground works such as highway and railway tunnels intersect with commercial farmlands or forested regions, especially in emerging countries as China

(Ouyang et al., 2018). As a result, drought instances have been observed on the high groundwater-dependent species in the low-land areas (Li et al., 2018). Therefore, any change on groundwater environment or any disturbance on the water balance of catchments may cause environmental impacts detrimental to surrounding vegetation. However, occurrences of these incidents are hard to predict because they depend on several environmental and hydrological factors (Jukaine et al., 1995; Rosenberg et al., 2000). Accordingly, it is essential to combine vegetative, atmospheric, and hydraulic parameter to address the occurrences of environmental impacts induced by tunnel drainage. Thus, reducing environmental impacts is a challenge from a tunneling perspective.

Previous studies that evaluate environmental impacts during tunnel excavation mostly focused on direct effects such as land hazards (Huang et al., 2015) and water contamination (Chae et al., 2008; Vik et al., 2000). Besides that, a few works focused on hydrological impact on groundwater environment from the drawdown perspective. Attanayake and Waterman (2006) introduced a method for the early detection of environmental impacts on water resources by observing groundwater table before and during the tunnel construction. Liu et al. (2015a) applied an indicator system to an existing tunnel project to estimate the degree

* Corresponding author.

E-mail address: lixiaojun@tongji.edu.cn (X. Li).

Nomenclature

b	shape-factor parameter for $R(\delta_r)$ (Eq. (A7)), dimensionless
ET	evapotranspiration, cm d^{-1}
$h = h(z, t)$	soil water pressure, cm
h^*	soil water pressure below which plants begin closing their stomata, cm
h_{\max}	soil water pressure value below which roots extract water at the maximum rate until h^* , cm
h_{\min}	allowable minimum soil water pressure at the soil surface, cm
h_w	soil water pressure below which plants begin to wilt, cm
I	canopy interception, mm
$K = K(h)$	unsaturated hydraulic conductivity, m s^{-1}
K_{eff}	effective hydraulic conductivity for layered soil profile, m s^{-1}
K_s	saturated hydraulic conductivity, m s^{-1}
m	empirical parameter in the soil retention function (Eq. (A6)), dimensionless
n	exponent in the soil water retention function, dimensionless
n^d	exponent in the soil water retention function on drying condition, dimensionless
n^w	exponent in the soil water retention function on wetting condition, dimensionless
P	precipitation, mm
PET	potential evapotranspiration, mm d^{-1}
$q_0 = q_0(t)$	initial surface flux, cm d^{-1}
q_0^*	normalized initial surface flux by K_s , dimensionless
q_{\max}	maximum constant surface flux, cm d^{-1}
$R(\delta_r)$	root length density distribution, cm^{-3}
R_{avg}	medium root length density, cm^{-3}
$S(z)$	root water uptake term, d^{-1}
S_e	effective saturation, dimensionless
$S_p = S_p(z)$	potential root water-uptake rate also referred to as the spatial distribution of τ over the topsoil, d^{-1}
t	time, d
t_0	time when simulation begins, d
t_1	initiation time of drawdown induced by tunnel discharge, d
t_2	the time water table stagnates and drawdown stops, d
z	vertical coordinate, cm
$z_b = z_b(t)$	water table level and lower boundary value, cm
z_d	depth of wetting front, cm
z_{\max}	depth of rock surface, cm
α	empirical parameter in the soil retention function (Eq. (A6)), d^{-1}
α_d	value of α for drying condition of the soil water retention function, d^{-1}
α_w	value of α for wetting condition of the soil water retention function, d^{-1}
α_{wt}	decline coefficient of water table (Eq. (3)), dimensionless
δ	rooting depth, cm
δ_e	effective rooting depth which represents 50% of the total rooting depth, cm
δ_r	relative root length normalized by δ , dimensionless
δ_w	the portion of the rooting depth which corresponds to h_w , cm
δ_w^*	the portion of the rooting depth which corresponds to h_w under condition that wetting front occurs ($= \delta_w - z_d$), cm

ε_0^*	normalized soil evaporation rate by q_0 , dimensionless
ε_c	canopy evaporation rate, cm d^{-1}
ε_s	soil evaporation rate, cm d^{-1}
$\theta = \theta(h)$	soil water content, m^3m^{-3}
θ_r	residual soil water content, m^3m^{-3}
θ_s	saturated soil water content, m^3m^{-3}
θ_s^d	saturated soil water content of the drying condition, m^3m^{-3}
θ_s^w	saturated soil water content of the wetting condition, m^3m^{-3}
$\mu(h)$	root water uptake as a function of soil water pressure, dimensionless
τ	potential transpiration rate, cm d^{-1}
τ_0	initial transpiration rate, cm d^{-1}
τ_0^*	normalized initial transpiration rate by q_0 , dimensionless
τ_a	actual transpiration rate, cm d^{-1}

of drainage impact on groundwater environment. Li et al. (2018) evaluated the potential environmental impacts of highway tunnel discharge based on groundwater table drawdowns considering the maximum rooting depth of pine trees growing in the vicinity of the tunnel. However, previous attempts for impact assessment neglected the availability of water in the soil above the groundwater table and drawdown was considered as the only parameter for establishing the assessment criteria. The magnitude of the drawdown that is critical for preventing environmental impacts on vegetative cover, and the period of time to reach the wilting point while being exposed to drawdown were not previously established. In order to assess the environmental impacts on vegetative cover, it is essential to focus on the dynamics of plant-available water in topsoil between the terrain surface and groundwater table.

Plant-available soil water content has a non-linear relationship with soil water pressure (suction pressure, h), depending on soil texture (Tietje and Hennings, 1996) and variability of soil texture (Yeh, 1989). It also depends on the infiltration rate and regional flow dynamics controlling the spatial variability of the groundwater table, as well as the associated capillary rise (Fan et al., 2017). Because the vadose zone acts as a buffer zone between groundwater and atmospheric forcing, soil water pressure is a concurrent parameter which interacts with atmospheric forcing (Granier et al., 2000; Norero, 1969), vegetation type, rooting zone (Fan et al., 2017; Yu et al., 2016), and groundwater level (Balugani et al., 2017; Miguez-Macho et al., 2008; Zhang and Schilling, 2006). Estimation of environmental impact on this critical zone with limited spatial information requires careful depiction of the physical factors mentioned above.

In this study, vulnerability is defined as the condition when soil water pressure reduces to the wilting point which is caused by tunnel discharge. From the perspective of environmental impacts and soil water dynamics, the wilting point is the final point where vegetation is not capable of extracting water from the soil (Furr and Reeve, 1945; Hendrickson and Veihmeyer, 1945; Kirkham, 2014). Numerical models were developed to address temporal Soil-Plant-Atmosphere continuum (SPAC) (Simmer et al., 2014) for deep and shallow groundwater tables (Romano et al., 1998; van Walsum and Groenendijk, 2008; Zeng and Decker, 2009; Zhu et al., 2012). Although previous studies focused on soil water pressure by stressing key factors (e.g., rooting depth, soil texture), the coupling of SPAC with groundwater table drawdown has rarely been evaluated.

This work aimed to propose a method to evaluate vulnerability conditions in a tunnel area by coupling topsoil water model with groundwater table drawdown. The method was used to diagnose the dynamics that drives the vegetation into wilting. We employed the vulnerability analysis on a specific case study to analyze whether the case is resilient to tunneling-induced drawdown.

The method has the following components:

1. Including a model of topsoil water pressure to simulate drawdown effect.
2. Parameterization of wilting dynamics and its integration into vulnerability.
3. Impact assessment representing a variety of groundwater table boundary conditions (BCs).

The paper is organized as follows: Section 2 provides site information, and Section 3 introduces the vulnerability assessment framework and defines the analysis criteria. Section 4 focuses on the dynamic behavior of wilting as an integral part of the framework, and presents the application of the vulnerability analysis for the study site, followed by discussion and conclusion in Sections 5 and 6, respectively.

2. Study site

This section provides information about our study site, including location, forest cover and vegetation, long and short term weather conditions, and relevant soil data.

2.1. Location and climate

The Mingtang Tunnel study site is located on Yuexi County, Anhui Province, mid-eastern China (Fig. 1a). The primary goal of the tunnel is to improve the connection between Hubei and Anhui provinces. The 7.548 km long tunnel runs in an east to west direction (266° – 272°). The tunnel has an average depth of ~ 435 m (Maximum: 548 m, minimum: 322 m.) below ground surface. The study area around the tunnel (180 km^2), as the part of the Mingtang catchment, corresponds to a deep fractured aquifer composed predominantly of moderately-weathered granite and gneiss, having three major faults along the tunnel axis (Chen et al., 2016; Li et al., 2016b, 2018). The topography is formed on wide concave valleys to the east and west by moderately steep escarpments, across a 300 m elevation on the tunnel area. Topography ranges from low (<300 m) to moderate (300 m–800 m), and high (800 m–900 m) elevations, which have relatively thinner soil with high organic content. The Mingtang region has a sub-tropical humid climate. Annual rainfall for the year of tunnel construction (2013–2014) was 946.4 mm with an average annual temperature of 14.5°C .

2.2. Land cover and soil

The region has been afforested from its original temperate deciduous cover to primarily mature Chinese Fir (*Cunninghamia Lanceolata*) and bamboo forests (*Phyllostachys pubescens*), and shrubs as understory species (Fig. 1b), with sparsely distributed farmlands, as is a typical practice in China (Minghe and Ritchie, 1999; Zhang et al., 2011b). An examination of a root profile to a depth of 1 m shows the typical forest structure in Anhui province (Zhang et al., 2011a). The highest grounds have sparse distribution of pine trees (*Pinus massoniana*, *Pinus Hwangshanensis*). Minor land use types consist of scattered built-up areas, high-ground tea plantations on terraced land, and partly irrigated agricultural land in valley bottoms. Most of the farmland along the corridor connecting the tunnel to highway is paddy field (*Oryza Sativa L*) where the surface is immersed in water for long periods. Some of the exploration boreholes encountered soft soil layers, mainly composed of silt, silty clay, and soft plastic clay with a thickness of 0.5–2.1 m. Soil parent material consists of residual clay minerals from fully weathered gneiss and relatively thin silty clay layers. Soil profiles down to rock bodies extend to more than ~ 20 m on some parts of the tunnel zone, according to borehole observations.

3. Vulnerability assessment framework and methodology

In this section, we introduced a practical assessment framework to evaluate the vulnerability of a region against tunnel discharge.

Components of framework is demonstrated and physical definition of vulnerability is made regarding to the key factors.

3.1. Assessment framework

Vulnerability analysis was conducted across the short-term by using limited data, which included information about the vegetation derived from literature, daily atmospheric readings, and typical soil profiles. The buffering capacity of topsoil was tested from a vulnerability aspect. We introduced the vulnerability assessment based on groundwater table drawdown and dynamic plant wilting (Section 3.3). From this, we introduce a simple preliminary method to inform future tunneling decisions from an eco-hydrological perspective. Fig. 2 shows a schematic diagram to summarize the preliminary vulnerability framework and data requirements. This framework contains three components: Modeling, data, and vulnerability analysis. As the principal element of the method, the vulnerability assessment framework allows us to test the occurrence of wilting of vegetation and the selected case study exceed the water limit. If both conditions are met, then the region would be deemed to be vulnerable to tunnel discharge of groundwater. The proposed framework includes evaluation of dynamic root zone wilting for local scale of the tunnel region.

3.2. Vulnerability criteria

We build our numerical experiment on the basis of permanent wilting point. Vulnerable conditions were specified for a wide range of wilting points based on the terrestrial vegetative cover (Kirkham, 2014). The permanent wilting point is the final point of the stress range where plants start to die off and represents soil and vegetation dependent water pressure limits, which are in a range of -5000 to $-200,000$ cm (~ 0.5 to -19.6 MPa) for a wide range of species (Slatyer, 1957). According to this definition, we defined the stomatal closure pressure, h^* , at -5000 cm and the average permanent wilting point, h_w , at -8000 cm (-0.79 MPa). First criterion is that any condition that lowers topsoil water pressure down to the wilting point is considered as vulnerable.

The depth that corresponds to the h_w of the root zone was called wilting depth (δ_w) and partially occupies the total root depth (δ). Therefore, partial drying of root depth was represented as the percentage ratio of wilting depth over the entire root depth ($[\delta_w/\delta]100$). Finally, the second criterion for vulnerability status can be summarized as $\delta_w/\delta > \delta_e/\delta = 0.5$.

The vulnerability assessment concludes depending on the outcome of the vulnerability analysis which is designed by incorporating dynamic root zone wilting (Fig. 2) to test vulnerability criteria. Dynamics of soil water pressure from topsoil model reveal wilting status as a function of time depending on defined boundary conditions.

3.3. Dynamics on root zone wilting

Following the general characteristics of the Mingtang area, a basic transient topsoil model was introduced in Appendix A. This section describes the transient numerical experiment based on the basic topsoil model to reveal root zone wilting dynamics.

3.3.1. Boundary conditions and model parameters

Upper (soil surface) and the lower (groundwater table) boundary conditions were imposed on the basic topsoil model for simulating the root zone. Constant soil water flux, q_0 , and initial pressure, h_0 , were defined as the prescribed boundary conditions for an isothermal homogeneous soil. Prescribed boundary conditions were defined for the upper:

$$q_{\max} = q_0 \text{ at } z = 0 \quad (1)$$

and the lower:

$$h(z, t) = 0 \text{ at } z = z_b = 5 \text{ m} \quad (2)$$

Partitioning of evapotranspiration (ET) was assumed in the range of Liu et al. (2015b) for sub-tropical temperate broad-leaved evergreen

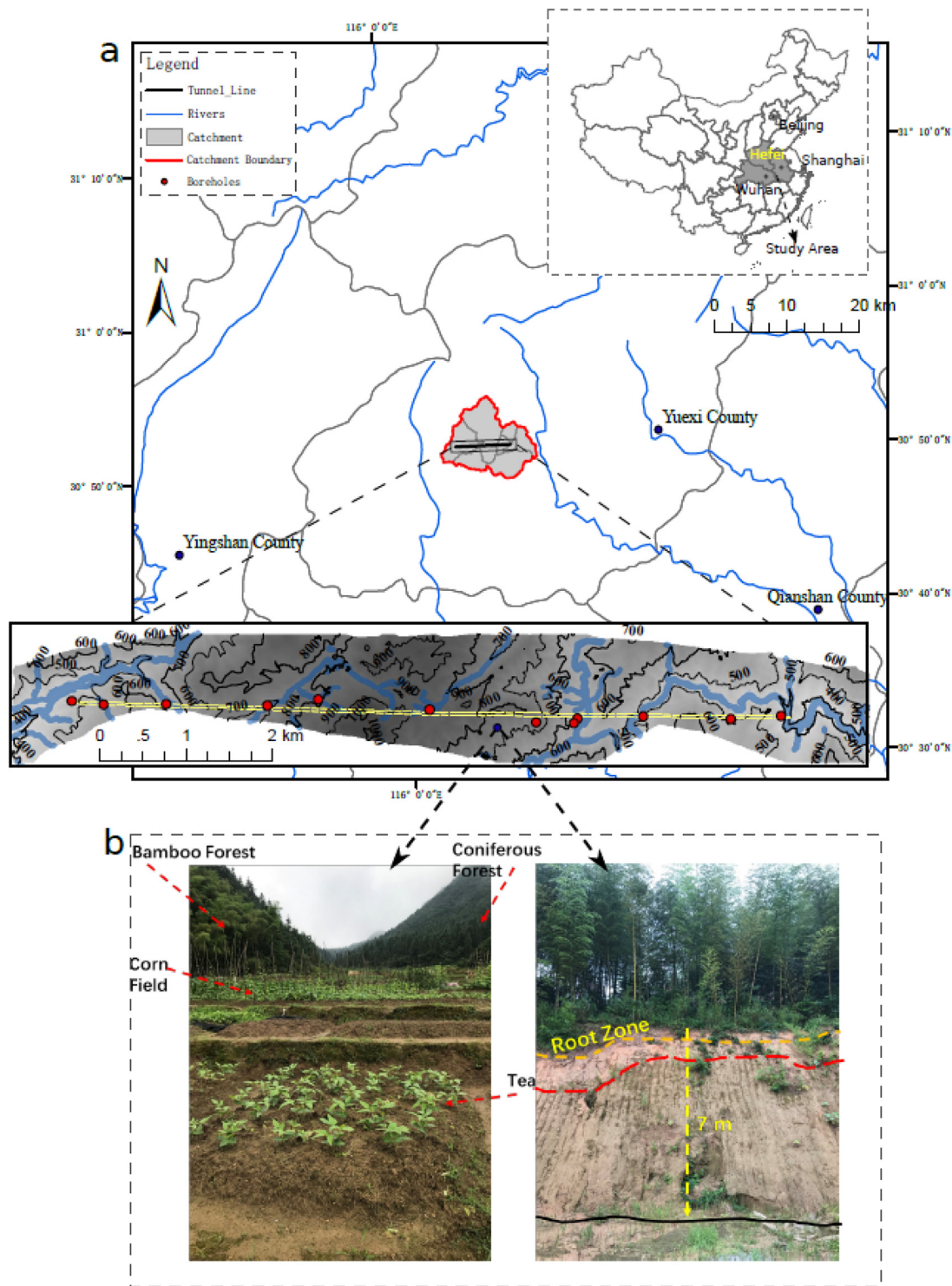


Fig. 1. Location and topography of the Mingtang tunneling area, where (a) the county and catchment that Mingtang tunneling was constructed on is demonstrated with a line under the approximate surface water network, and (b) bamboo and Chinese fir forests as two dominant kinds of vegetation cover. Cultivated fields located on high ground are shown in the left picture, and a typical soil profile is shown in the right picture with a root zone, upper loamy clay and bottom clay layers.

forest in which a large portion of the forest cover was composed of pine trees. Thus, the annual partitioning ratio was set to be 8% for soil evaporation (ϵ_s) and 60% for transpiration rate (τ) while total ET was kept constant (Table 1). According to Eq. (A1), the balance for wilting which is $P - \epsilon_c < \tau + \epsilon_s$ was evaluated to satisfy wilting conditions.

The unsaturated model was implemented for two single profiles with 20 m thickness; sandy-loam (high saturated conductivity,

$K_s = 106$ cm/d) and clay-loam (low saturated conductivity $K_s = 3.6$ cm/d) soil domains.

Model parameter values are listed in Table 2. Homogeneous soil settings were used for root zone wilting analysis with clay-loam and sandy-loam soil textures. Suction in specified conditions was modeled by the inclusion of the hysteresis model (Lenhard et al., 1991). Hysteretic soil-water characteristic curves for wetting and

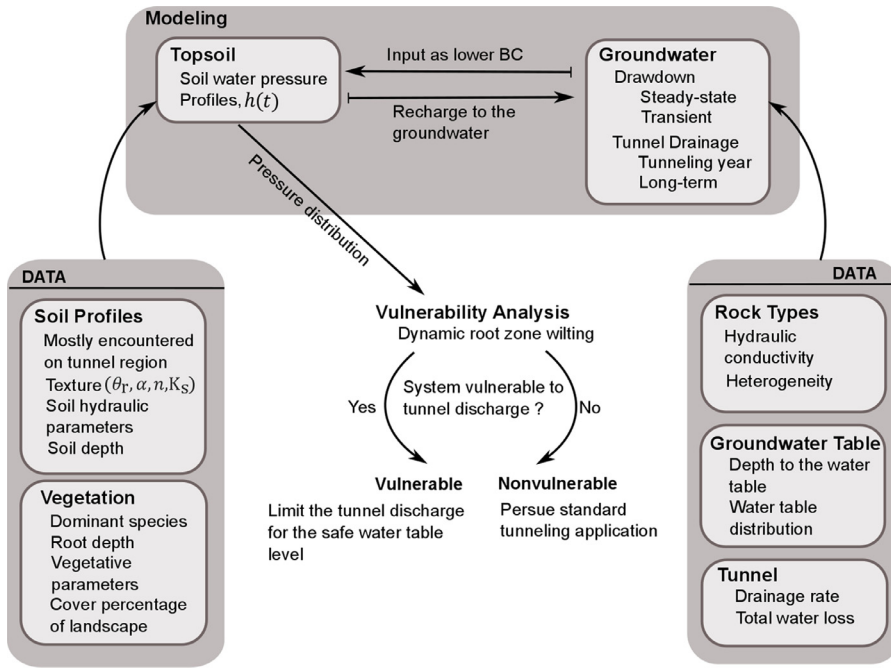


Fig. 2. Schematic outline of suggested preliminary vulnerability assessment process.

Table 1

Assigned boundary values for two soil textures. Relative rates (Unitless) q_0^* , τ_0^* and ϵ_s^* represent the normalized q_0 over K_s ($=q_0/K_s$) and, τ_0 , ϵ_s over q_0 ($=\tau_0/q_0, =\epsilon_s/q_0$ in turn). All other rate units are in cm d^{-1} .

Partitioning	Constant boundary values					
	q_0^*	$q_0(\text{cm d}^{-1})$	τ_0^*	$\tau_0(\text{cm d}^{-1})$	ϵ_s^*	$\epsilon_s(\text{cm d}^{-1})$
Loamy clay	0.001	0.0036	3.5	0.0126	0.48	0.00168
Sandy Loam		0.106		0.382		0.051

drying conditions were represented by the ratio of soil-water retention parameters (Nielsen and Luckner, 1992; Parker and Lenhard, 1987; Šimůnek et al., 2013). The ratio of wetting and drying parameters were assumed as $\alpha_w/\alpha_d=2.24$, $n^w/n^d \sim 1$, and, wetting and drying saturated water contents ratio was set as $\theta_s^w/\theta_s^d = 0.9$ based on the experiments conducted on a wide range of soil types (Likos et al., 2014).

The medium root density, R_{avg} , ($=0.1 \text{ cm}^{-3}$) and shape-factor parameter, $b(=2)$ were applied using previously published distribution parameters (de Jong van Lier et al., 2006; Santos et al., 2017). Seasonal variations of rooting depth and root density were not considered. Rooting depths were assumed to be in the range 40–340 cm, based on *ex-situ* information (taken from the compiled data from the literature, see appended research data), corresponding to the maximal and minimal values of rooting depths of temperate mixed coniferous and bamboo forests (See Section 2). Thus, the rooting depth was assumed to be the mean root depth of 100 cm for the base conditions. Each soil

profile, $R(\delta_r)$ (Eq. (A7)) was designed such that about 80% of the total root mass occupied the top portion of the soil (Yu et al., 2007; Zhuang et al., 2001), which represents the effective root depth.

The wilting process was simulated for a long time by 1 to 5-day intervals depending on the spatial wilting rate (for the pressure field) and demonstrated until vulnerability criteria are met (See Fig. 3).

3.3.2. Integration of vulnerability criteria with root zone wilting behavior

Results of the transient root zone pressure distributions are illustrated in Fig. 3, which shows the simulated wilting behavior with the same relative infiltration rates and a constant groundwater table level for two soil textures. Each pressure distribution represents a specific day. Early day pressure profiles represent relatively wetter soil than the following days until wilting conditions prevail. The results are interpreted to parameterize the behavior of wilting and generalize the physical dynamics of the vulnerability.

The wilting process is not uni-directional, it initiates at the effective rooting depth ($z \sim \delta_e$) and spreads over two directions simultaneously (Fig. 3). A wetting front (z_d), where infiltration prevails against transpiration and evaporation, limits wilting close to the soil surface. Therefore, we redefine the wilting depth as a modified wilting depth (δ_w^*), which is the depth after the subtraction of the wetting front depth ($\delta_w^* = \delta_w - z_d$).

Dynamic wilting analysis of root zone suggests that wilting was initially observed between $z = 10$ and 20 cm after 1260 days, and reached the vulnerable point ($\delta_w^* > \delta_e$) on the 2060th day for clay-loam (Fig. 3a). Root zone wilting occurred between the 1560th and 2060th day.

Table 2

Representative soil profile for approximate layered topsoil profile reported during preliminary survey for Mingtang tunnel.

Soil type	Depth (cm)	Bulk density (g cm^{-3})	θ_r ($\text{cm}^3 \text{cm}^{-3}$)	θ_s ($\text{cm}^3 \text{cm}^{-3}$)	α (cm^{-1})	n	K_s (m s^{-1})	K_{eff} (m s^{-1})
Clay loam ^a	0–60	1.40	0.095	0.410	0.019	1.31	7.222E–07	2.311E–07
Clay ^a	60–160	1.40	0.068	0.380	0.008	1.09	5.556E–07	
Silty clay ^a	160–340	1.40	0.070	0.360	0.005	1.09	5.556E–08	
Clay ^a	340–1500	1.40	0.068	0.380	0.008	1.09	5.556E–07	

^a Class average values for van Genuchten’s (1980) model from Carsel and Parrish (1988).

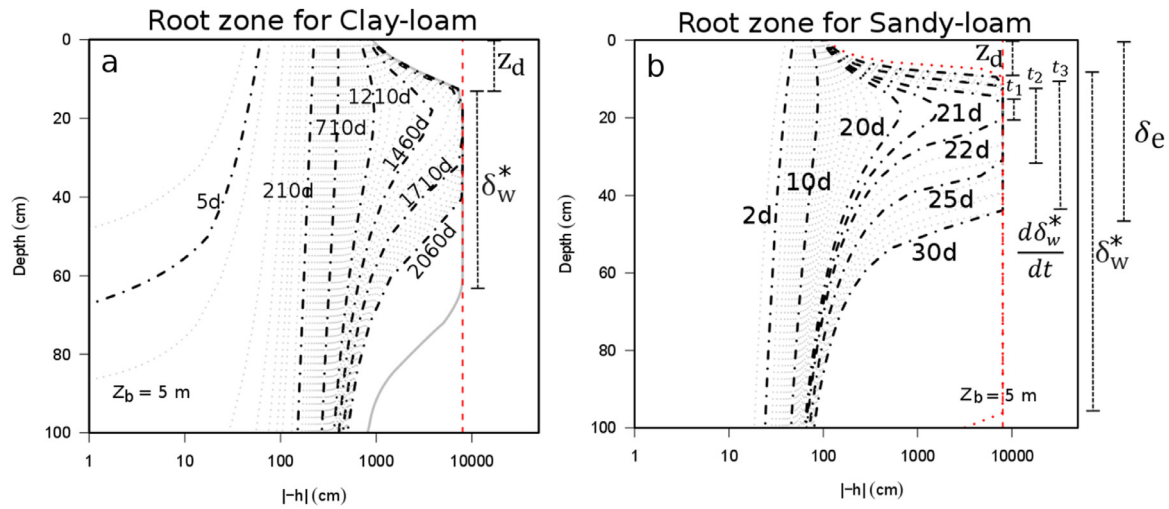


Fig. 3. Numerical experiment results and visual parameterization of soil water pressure for dynamic root zone wilting in the upper 100 cm of the soil. Graphs demonstrating transient soil water pressure profile changes on rooting zone until wilting condition is met, during the period towards the equilibrium (a) for clay-loam and (b) sandy-loam textures. Condition of $z_b = 5$ m is presented for both profiles as wilting conditions. Discontinuous lines demonstrate pressure distribution for each designated time. General behavior is highlighted with dark discontinuous lines with reported days. Wilting parameters introduced as the evaluation of wilting depth (δ_w^*) shown as representative times ($t_1 = 22d$, $t_2 = 25d$, $t_3 = 30d$) on sandy-loam texture. Assumed effective root depth (δ_e) is also noted for schematic comparison. Wetting fronts (z_d) are demonstrated for both textures.

Because the presence of wetting front limited the upward movement of the wilting point, δ_w^* occupied approximately 52% of the root zone (52 cm) at equilibrium, which corresponds to wilting on the whole δ_e . The wilting process happened between the 21st and 30th day (Fig. 3b) for the sandy-loam soil, similar to the dynamics of wilting in the clay-loam soil. Conversely, δ_w^* extended to 90% of the root zone (~90 cm) and satisfied the vulnerability criteria. However, the 30-day profile did not represent vulnerability conditions since δ_w^* occupied 37% of the root zone.

4. Vulnerability assessment of the study-site

We aimed to capture the impact of early drawdown using the deep groundwater model (Li et al., 2018) shown in Fig. 4. The groundwater level initially dropped to 15 m but then recovered after 20 days. After the recovery, maximum drawdown remained at approximately 7.5 m within the 300-day period as a result of groundwater recharge. We tested the impact of this behavior on a selected case study at 200 m distance from the Mingtang tunnel area which contains nearly saturated layered soil profiles with a shallow groundwater table ($z_b(t_1) = 1.2$ m). The following sections explain the model design (Section 4.1), soil profiles and details of specific case study (Section 4.2), and simulation results (Sections 4.3 and 4.4).

4.1. Model design and variable drawdown condition

A variable lower BC was imposed on the unit profiles in order to represent time-dependent groundwater table drawdown. We used a simple transient drawdown model introduced by Zhang and Schilling (2006). The model is summarized as follows:

$$z_b(t) = z_b(t_1) - z_b(t_2)(1 - e^{-\alpha_{wt}t}) \quad (3)$$

where $z_b(t)$ is the transient water table depth after the elapse of time t , $z_b(t_2)$ is the asymptotic depth at which the groundwater table becomes stable, α_{wt} is the decline coefficient (Fig. 5). Here, selection of α_{wt} should be made carefully to determine a realistic variation in depth to the water table. BC was defined as:

$$h(z, t) = 0 \text{ at } z = z_b(t), t_1 < t < t_2. \quad (4)$$

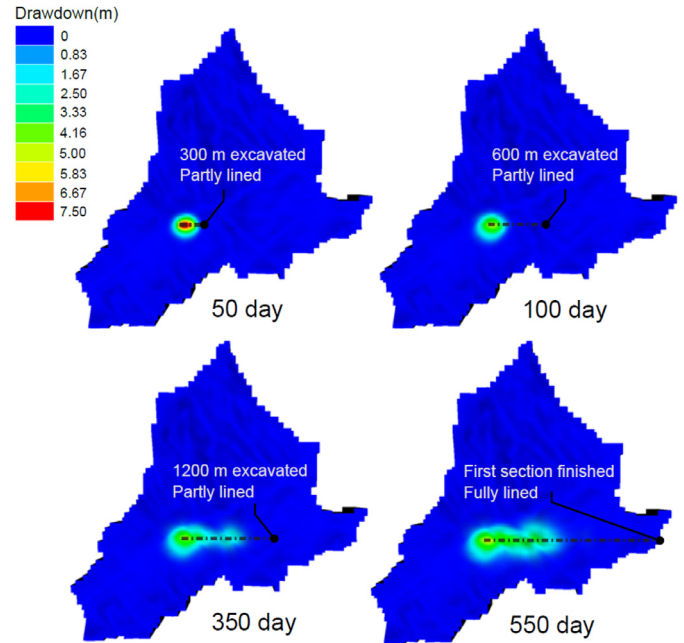


Fig. 4. Transient deep groundwater table alterations during construction of the Mingtang tunnel. This Figure demonstrates the water table distributions from the beginning of the construction until the end of the first section where initially there was a high water table recession followed by recovery after tunnel construction was completed (550 days). According to groundwater simulations water table drop down to 15 m in the first 10 days.

where t_1 and t_2 are the initiation time of drawdown and the designated period after drawdown has finished, respectively; $z_b(t_2)$ was set to be the highest saturated depth ($z_b(t_2) \cong 15$ m) for the 10-day simulation and initiated at $z_b(t_1) = 1.2$ m based on transient deep groundwater model simulation results in Fig. 4 (For details see Li et al. (2018)). We formulated three scenarios depending on drawdown rates: fast, $\alpha_{wt} = 1.0(t^{-1})$, moderate, $\alpha_{wt} = 0.2$, and slow, $\alpha_{wt} = 0.1$. On the 10th

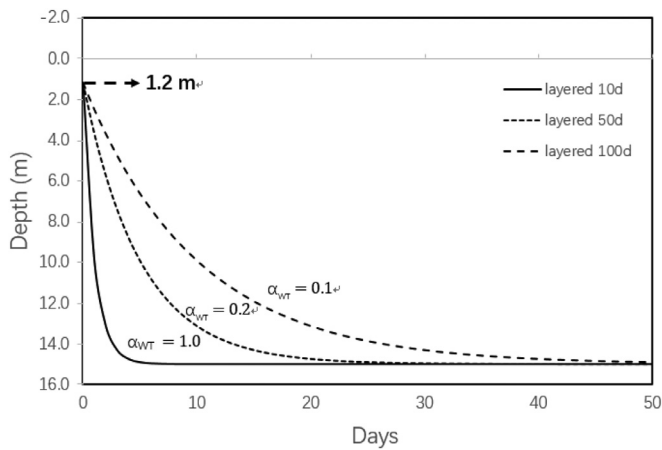


Fig. 5. Time dependent water table recession curves based on different draw-down rates, α_{WT} . The curves represent the variable water table ($z_b(t)$) boundary conditions for the case study. $z_b(t_1)$ was set to 1.2 m for the layered profile. Boundary conditions represent the initial 50 days of groundwater tunneling where the impact of drawdown was expected to be higher.

day, the fast rate curve leads to 15 m, moderate and slow curves occur at 12.5 m and 8.9 m groundwater table depths, respectively. The shift was demonstrated for the layered soil profile down on 15 m and simulations were extended for 300 days.

4.2. Soil profile

The heterogeneous soil profile, which is widely seen on study-site, with layered soil properties was introduced (Fig. 6). In this work, soil heterogeneity is restricted to K_s associated with each layer on one-dimensional vertical domain. The layered soil profile was formulated with a shallow groundwater table, which was assumed to exist on the low-land section of the Mingtang tunnel. The profile was composed of loamy clay and silty mixture over a thick clay layer (Table 2). ET was selected as 0.54 cm/d by averaging weather data and calculated using the Penman–Monteith equation (Monteith, 1997). The average partitioning ratio was estimated from transient atmospheric BC as $\tau/PET \sim 0.75$, which is equivalent to a total evaporation of 0.13 cm/d. Rooting depth, δ , was assumed to be ~ 100 cm. The water table depth was set to 1.2 m below the soil surface as a safe condition for pine forest cover (dominantly *Pinus massoniana*, *Cunninghamia lanceolata*) based on feasibility reports from the Shanghai–Wuhan Expressway project.

4.3. Dynamic root zone wilting above the tunnel area

In this section, our general focus is to test the effect of tunnel discharge induced drawdown on the vicinity of tunnel area. Groundwater recharge from topsoil was omitted and thus the recovery of the groundwater table was not included. Fig. 7 shows the time-dependent response of the topsoil to the drawdown. Groundwater table drawdown reached the fixed level on different times depending on α_{wt} . For the layered profile, the difference between pressure distributions was identical due to drawdown rates, therefore pressure profiles for only one rate is presented. For all the other rates, pressure profiles for variable drawdown rates are demonstrated in Fig. B.1.

4.4. Impact of heterogeneity on dynamic root zone wilting

The equivalent homogeneous profile was formulated based on effective hydraulic conductivity, K_{eff} (Table 2), which is the perpendicular saturated hydraulic conductivity and equals the harmonic mean

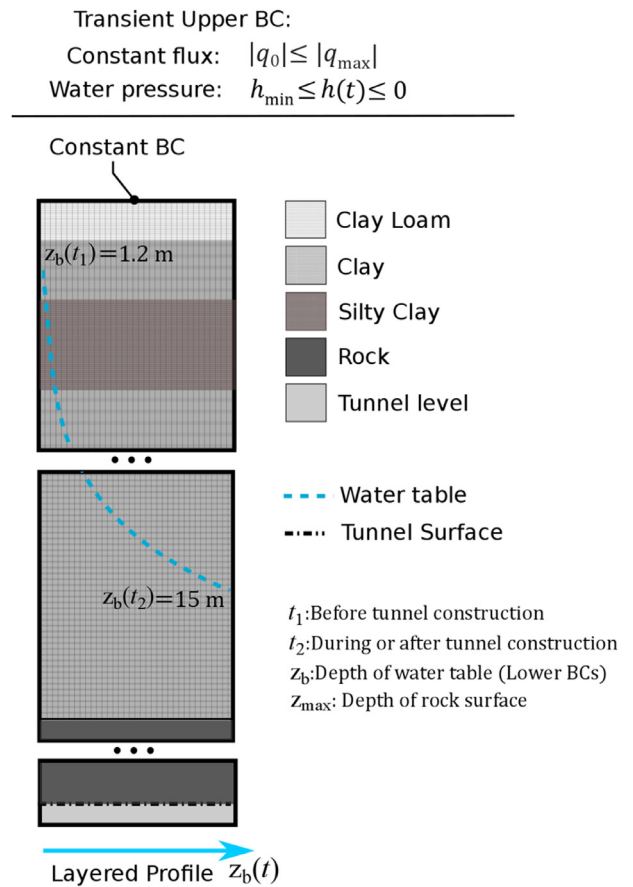


Fig. 6. Summary of 1D Unit soil profile for a layered soil with imposed upper and lower boundary conditions (BC). Profile represents the heterogeneous soil profile of case study with variable groundwater table BCs without infiltration. Variable groundwater table BCs ($z_b(t)$), is demonstrated between the initial, $z_b(t_1)$ and final water table levels, $z_b(t_2)$. Previously specified root water uptake function and root length density distribution were also valid. For this study atmospheric BC is neglected for layered and equivalent homogeneous profiles, instead average values are imposed as constant BC.

of hydraulic conductivities for each layer in the layered soil profiles (Sanchez-Vila et al., 2006). K_{eff} value for the layered soil profile was close to that for a sandy-clay texture, which was therefore selected for the equivalent homogeneous profile (Carsel and Parrish, 1988). Same BCs of layered soil profile was imposed on the homogeneous soil profile. BCs are summarized in Fig. 6.

Results were compared with the equivalent homogeneous soil profile to observe the impact of one-dimensional heterogeneity. Different drawdown rates did not lead to different water pressure profiles (Fig. B1). Therefore, in Fig. 7, only profiles of the slow drawdown rate are presented. Groundwater table drawdown does not correlate with topsoil dynamics directly, and the saturated zone persisted between 0.6 m to 1.9 m. In contrast to the homogeneous soil profile (Fig. 7b), the connection between the deep saturation zone and root depth was not disturbed by a low permeability layer (silty-clay), but this did not limit the development of root wilting. Neither the heterogeneous soil profile nor the equivalent homogeneous soil profile exhibited wilting conditions in the first 10 days. The heterogeneous profile (Fig. 7a) water pressure drained down to the wilting pressure in 11 days. From the 11th day, water pressure decreased to the wilting point, and the vulnerability criteria were satisfied, ($\delta_w = \delta_e$) on the 220th day in the layered soil. However, the vulnerable condition occurred on the 300th day in the homogeneous profile (the gray area in Fig. 7a and b).

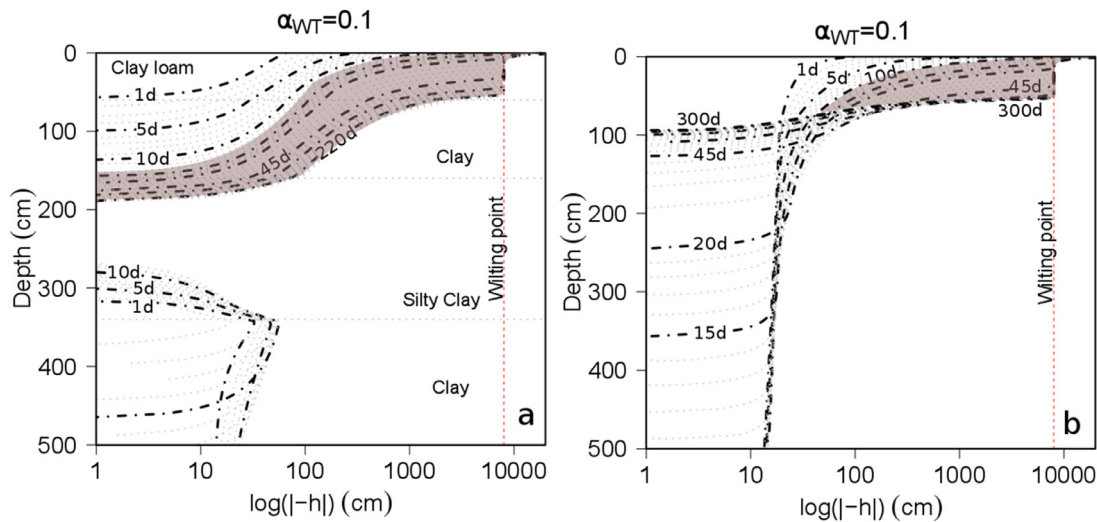


Fig. 7. Dynamic root zone wilting for (a) layered, and (b) homogeneous profiles equivalent to the layered soil profile, by demonstrating transient water pressure profiles. Pressure profiles are shown with the corresponding time in the 300-day period. Pressure curves were demonstrated until the vulnerable condition was attained. Numbers on the curves represent the occurrence day of the pressure profile. The gray area highlights the curves that induce wilting. (For interpretation of the references to color in this figure legend, the reader is referred to the web version of this article.)

Overall, root zone pressure levels varied independently of the rate of drawdown and, this varied due to heterogeneity of soil types.

5. Discussion

5.1. Root zone under vulnerability conditions

The results of analyses of dynamic wilting (Fig. 3) based on numerical experiment, suggest that the wilting process is not a straightforward phenomenon. Rather, it requires interpretation across time to integrate with the vulnerability assessment framework. The wilting process continues until the root wilting depth, δ_w (δ_w^* in the case of the wetting front), reaches at least 50% of entire root depth. In general, δ_w depends on z_b and soil texture. Therefore, a deep water table may not lead plants to wilt in fine texture soils, which have a large capacity to store plant-available water. Conversely, δ_w may occupy the entire effective root depth under conditions of a shallow water table for coarse texture soils. Regarding a single z_b (5 m), dynamic root zone analysis proves that rainfall occurs, the wilting process does not initiate directly from the soil surface, but at a depth of ~ 30 cm for both textures, and δ_w^* extends down to the root zone until pressure equilibrium is satisfied. The water pressure in the upper part of the root zone never decreased to the wilting point because of the wetting front that existed within the upper part of the soil profile. Finally, independent of soil texture, a sufficient amount of rainfall-induced infiltration can secure the water content of the upper part of the root zone, and this may neutralize the effect of groundwater drawdown.

In the dynamic wilting analysis, wilting time differs depending on soil texture. As expected, wilting on a clay-loam profile was substantially slower than on a sandy-loam soil. However, in reality, infiltration rates vary independently of K_s , depending on rainfall intensity. Based on the imposed BCs, transpiration rate of the clay-loam (Table 1) was relatively insignificant, and this may not indicate vulnerability. As seen from the impacts of atmospheric BCs, variable rates of PET and P may change the wilting behavior, as having K_s values lower than clay-loam and clay. In the long term, plant roots and root distribution changes as well as the other vegetative parameters (Chaves et al., 2003; Taylor and Klepper, 1979). However, we have not included root growth dynamics in the topsoil model. Therefore, the clay-loam soil profile is least likely to reach the state depicted in Fig. 3.

5.2. Impact on vulnerable case: shallow groundwater table soil

We checked the assumption by Li et al. (2018) which suggested that the highest drawdown that arose was approximately 15 m and that this occurred after the initiation of tunnel drainage (Fig. 4) to examine the impact probability. To test the assumption from vulnerability perspective, a layered soil profile with a shallow water table located on a low-land area was specified and compared with their equivalent homogeneous soil. Our findings suggest that topsoil water pressure behaves independently of groundwater drawdown. An indication of wilting was not present for the initial 10 days. Furthermore, the rate of drawdown did not affect topsoil pressure for daily time scale. In general, topsoil water pressure was reduced throughout the duration of the 300-day simulation. However, the vulnerability criteria were not being met for a long time, which is an indication that the plant-available moisture content for Mingtang soil was independent of groundwater drawdown during the early phase. The response of the root zone differs according to the heterogeneity of the soil profile, thus the response depended on the order of the layers. The layered soil profile was composed in such a way that the higher K_s clay layer was located above the lower K_s silty-clay layer, and thus the upper layer maintained the supply of plant-available water and increased the resistance of pine trees to early wilting. The perched water condition (Kelln et al., 2009) created a delay in the drying process induced by groundwater table drawdown, (Fig. 7a), where the silty-clay layer inhibited any decrease in the saturated water level. Consequently the topsoil water pressure behaved differently according to the varying texture of the soil (Yeh, 1989). The homogeneous soil profile in the case study demonstrated the development of the wilting condition in different way (Fig. 7b), where wilting conditions were met with a delay. The difference of the wilting dynamics proved that the wilting process is dependent more on soil heterogeneity than BCs. Therefore, soil heterogeneity is a factor that should be carefully addressed which effects the vulnerability assessment results.

5.3. Preliminary framework for impact control

The environmental impact from tunneling perspective is mostly considered as acute effects during construction periods such as pollution or land hazards (e.g., ground settlement). However, we claim that long-

term discharge from the tunnel is critical for regional water budget, which is directly affected by atmospheric changes and fluctuations of groundwater. Any discharge level cannot be compensated by the water resources of a local environment for a certain duration of time (e.g., a year or more) leads incremental adverse effects on the environment thus may exceed the impact of acute effects. Therefore, the region would be classified as vulnerable. The main purpose of the assessment framework is to give preliminary insight for decision makers about the vulnerability of a region against tunnel discharge. We designed a simple method that provides sufficient information with the help of numerical models. Outcomes of dynamic root zone wilting analysis proved that the assessment is successful in linking discharge impact and physical modeling.

In this study, we have conducted vulnerability analysis on a hypothetical case study based on real study-site for a short period (up to 300 days), however, we did not include atmospheric changes and focused on dynamic wilting concept. It is imperative to extend the analysis to decadal time scales to have a better evaluation of the environmental impact by changes to local weather conditions. Extension of the vulnerability analysis of the proposed framework may provide the impact of long term atmospheric alterations on vulnerability. The framework has the potential to apply regionally to classify locations that are vulnerable to tunnel discharge. The precision of assessment can be increased by having more detailed soil profiles and vegetation data.

6. Summary and conclusion

This study introduces a vulnerability assessment framework by coupling topsoil water model with deep-tunnel discharge. Soil water pressure was introduced as a new performance metric for the vulnerability analysis in the unsaturated zone above groundwater table. Accordingly, vulnerability criteria were defined by combining plant wilting and water pressure distribution. Dynamic root zone wilting process was performed to parameterize vulnerability via transient unsaturated flow simulation. Theoretical case study was presented to demonstrate the application of vulnerability analysis for layered soil and vegetation cover.

Analysis results for the study-site showed that drawdown larger than the root zone depth alone did not satisfy vulnerability criteria. Transient groundwater table drawdown on topsoil did not manifest vulnerable conditions before the 220th day of the simulation. Case study results demonstrated that the development of wilting in such occasions depended on the boundary conditions and the formation of the soil types, with deep water levels being independent of the rate of tunnel discharge. The equivalent homogeneous pressure profile results showed different vulnerability status than observed in the layered soil simulation with a delay of wilting time.

The study presents deeper insight into potential environmental impacts induced by deep tunnel drainage. Our future study will focus on the improvement of the vulnerability assessment by integrating atmospheric forcing and the climatic factors into the framework.

Acknowledgments

The research was conducted with support from the [Natural Science Foundation of China](#) (Grant no. 41877246), the Science and Technology Plan Project of the [Ministry of Transport of China](#) (2013318J02120), the Tongji Civil Engineering Peak Discipline Plan, and the Fundamental Research Funds for Central Universities.

Appendix A

This appendix explains the design and assumptions of the basic transient topsoil model and root water uptake.

A.1. Transient topsoil model

The basic model setting was initiated as a transient solution of unsaturated flow for a homogeneous soil profile (Fig. A1). The model

was designed to represent the Soil-Plant-Atmosphere continuum coupled with a tunnel-discharge-induced groundwater table drawdown. Root zone wilting could be assessed by analyzing transient root zone pressure profiles, in which the transition of water pressure into h_w was observed. More theoretical cases could be introduced by increasing model complexity over the basic model.

In the basic model, the water balance of the critical zone, namely the zone between saturated water level and terrain surface or vadose zone, is described by:

$$q_0 = P - I - ET = (P - \varepsilon_c) - \varepsilon_s - \tau \quad (A1)$$

where, in the absence of surface runoff, q_0 is the initial soil water flux, P is daily precipitation, ET and I stand for potential evapotranspiration and relative canopy interception, respectively. As the parameters to characterize partitioning, ε_c and ε_s represent canopy and soil evaporation, respectively. It was assumed that all canopy interception is equivalent to ε_c , meaning all intercepted rainfall evaporates from the vegetation canopy. τ is transpiration rate of the associated vegetative cover, which is modeled as a function of rooting depth.

Soil water pressure distributions were simulated with Hydrus 1D (Šimůnek et al., 2013). The vadose zone was physically modeled by using the Richards equation to simulate unsaturated flow as:

$$\frac{\partial \theta(z)}{\partial t} = \frac{\partial}{\partial z} \left[K(h) \left(\frac{dh}{dz} + 1 \right) \right] - S(z), \quad (A2)$$

where z denotes vertical coordinate, $\theta(z)$ represents water content, h is the soil water pressure, and $K(h)$ is the unsaturated hydraulic conductivity. $S(z)$ is the root water uptake term integrated with the method proposed by Feddes (1978), summarized as:

$$S(z) = \mu(h) S_p(z) \quad (A3)$$

where $S_p(z)$ is potential root water-uptake rate ($L^3 L^{-3} T^{-1}$) and $\mu(h)$ is a dimensionless, stepwise water pressure response function (Šimůnek et al., 1992), summarized below:

$$\mu(h) = \begin{cases} 0 & h \leq h_w \\ (h - h_w) / (h^* - h_w) & h_w < h < h^* \\ 1 & h^* < h \end{cases}, \quad (A4)$$

where h_w is the wilting point pressure and h^* represents the point of stomatal closure. The function regulates root water uptake as plants cease to extract water below h_w ($\mu(h) = 0$). Above h_w , root water uptake increases linearly up to h^* as the soil gets wetter. Conditions at which water pressure exceeds h^* represent the maximum rate of uptake.

Unsaturated hydraulic conductivity, $K(h)$, was modeled using the Mualem-van Genuchten soil hydraulic model with an air entry (bubbling) pressure of -2 cm (van Genuchten, 1980; Mualem, 1976):

$$K(h) = K_s S_e \left[1 - \left(1 - S_e^{1/m} \right)^m \right]^2, \quad h \leq 0 \quad (A5)$$

$$S_e = \frac{\theta(h) - \theta_r}{\theta_s^j - \theta_r}$$

where K_s is saturated hydraulic conductivity; S_e is effective saturation; m is an empirical parameter; θ_s^j and θ_r are saturated and residual water contents, respectively; $\theta(h)$ is volumetric moisture content as a function of water pressure. The soil-water characteristic release curve $\theta(h)$ is given by:

$$\theta(h) = \begin{cases} \theta_r + \frac{\theta_s^j - \theta_r}{[1 + \alpha_j h^{n_j}]^m}, & h < 0 \\ \theta_s, & h \geq 0 \end{cases} \quad (A6)$$

where α_j , n_j , and $m (= 1 - 1/n_j)$ are empirical parameters for each specified soil texture. The subscript j is by either w or d , corresponding to wetting or drying cycles, respectively.

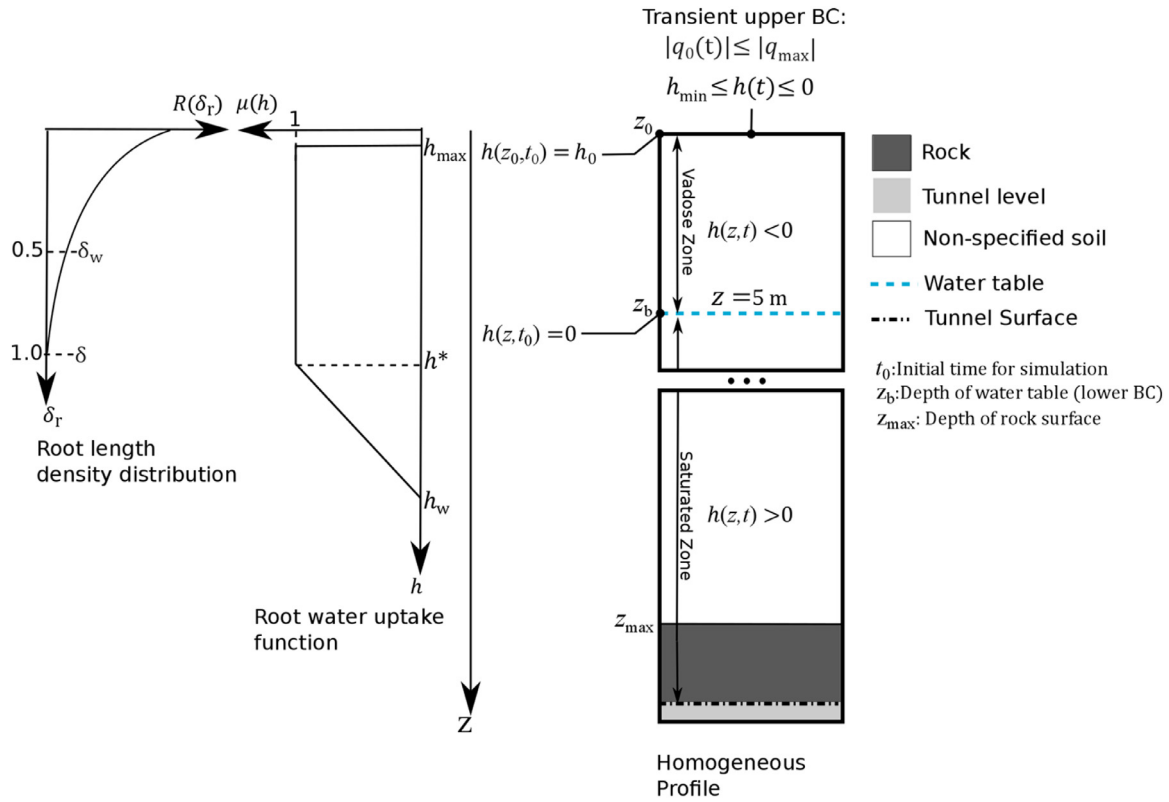


Fig. A1. Base 1D unit soil profile for a homogeneous soil profile. This includes vegetative information as root length density distribution, $R(\delta_r)$, and root water uptake as a function of soil water pressure $\mu(h)$. Designated boundary conditions for the transient model over the underground tunnel are summarized. Saturated and vadose portions of homogeneous soil profile are demonstrated schematically with groundwater table (z_b) boundary conditions. (For interpretation of the references to color in this figure legend, the reader is referred to the web version of this article.)

A.2. Design of root water uptake

Rooting systems were designed using the Santos model (see below), where the vegetation assumed to be fully grown and root has not been truncated by any solid obstacle. Water uptake along the rooting depth δ was controlled by root density distribution function, which is modeled as follows (Santos et al., 2017):

$$R(\delta_r) = \frac{b^2 R_{avg}}{b + \exp^{-b} - 1} (1 - \delta_r) \exp^{-b\delta_r} \quad (b > 0). \quad (A7)$$

where $R(\delta_r)$ is root specific length (defined as root length per unit bulk soil volume) distribution as a function of the relative depth $\delta_r (= z/\delta)$, R_{avg} is root density, b is a shape-factor parameter. The potential root water-uptake rate $S_p(z)$ is normalized as:

$$S_p(z) = \frac{R(\delta_r)}{\int_0^1 R(\delta_r) d\delta_r} \tau \quad (A8)$$

Root density distribution was assigned assuming that roughly 70% of the plant's water supply is provided by the upper 50% of the total rooting depth, which we have called the effective rooting depth (δ_e) (Bennett and Doss, 1960). Root water uptake ceases irreversibly once water pressure within δ_e completely reduces to the wilting pressure, h_w . Water uptake is arranged in such a way that the plants would immediately start to extract water at a maximum rate when soil water pressure h is less than -1 ($h_{max} = -1$), and remains at this maximum rate until h reduces to stomatal pressure, h^* , and then diminishes linearly to zero at h_w . The root water uptake function is shown in Fig. A1. Actual water uptake behaves as a function of pressure distribution, as shown in Eq. (A4), and represented by $\mu(h)$.

Appendix B

Figs. A1 and B1.

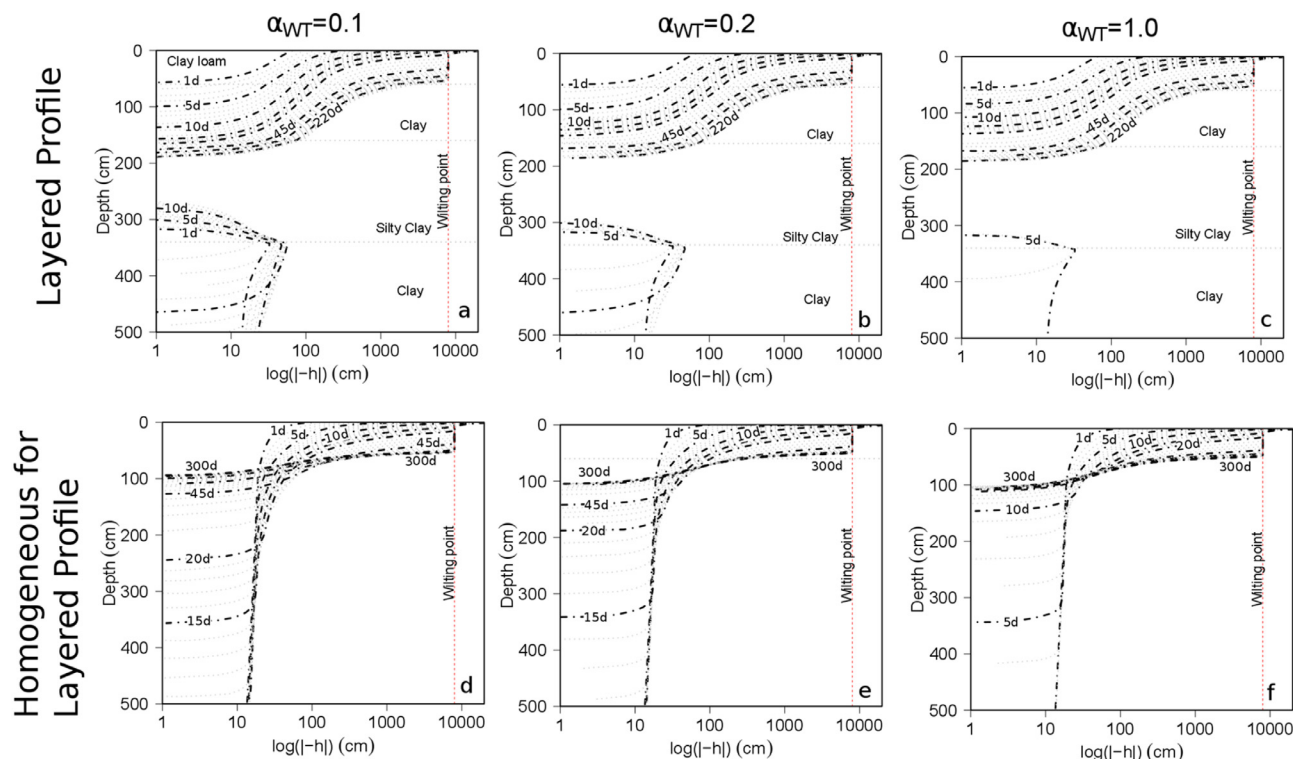


Fig. B1. Transient demonstration of the pressure profiles to compare layered soils (a–c) with homogeneous soils for layered (d–f), and for paddy fields (g–i). Each column represents the pressure profiles of different rates of drawdown.

References

- Attanayake, P.M., & Waterman, M.K. (2006). Identifying Environmental Impacts of Underground Construction, (January). <https://doi.org/10.1007/s10040-006-0037-0>.
- Balugani, E., Lubczynski, M.W., Reyes-Acosta, L., van der Tol, C., Francés, A.P., Metselaar, K., 2017. Groundwater and unsaturated zone evaporation and transpiration in a semi-arid open woodland. *J. Hydrol.* 547, 54–66. <https://doi.org/10.1016/j.jhydrol.2017.01.042>.
- Bennett, O.L., Doss, B.D., 1960. Effect of soil moisture level on root distribution of cool-season forage species. *Agron. J.* 52, 204–207. <https://doi.org/10.2134/agronj1960.00021962005200040008x>.
- Butscher, C., Einstein, H.H., Huggenberger, P., 2011. Effects of tunneling on groundwater flow and swelling of clay-sulfate rocks. *Water Resour. Res.* 47 (11), 1–17. <https://doi.org/10.1029/2011WR011023>.
- Carsel, R.F., Parrish, R.S., 1988. Developing joint probability distributions of soil water retention characteristics. *Water Resour. Res.* 24 (5), 755–769. <https://doi.org/10.1029/WR024i005p0755>.
- Cesano, D., Olofsson, B., Bagtzoglou, A.C., 2000. Parameters regulating groundwater inflows into hard rock tunnels – a statistical study of the Bolmen tunnel in southern Sweden. *Tunn. Undergr. Space Technol.* 15 (2), 153–165. [https://doi.org/10.1016/S0886-7798\(00\)00043-2](https://doi.org/10.1016/S0886-7798(00)00043-2).
- Chae, G.-T., Yun, S.-T., Choi, B.-Y., Yu, S.-Y., Jo, H.-Y., Mayer, B., et al., 2008. Hydrochemistry of urban groundwater, Seoul, Korea: the impact of subway tunnels on groundwater quality. *J. Contam. Hydrol.* 101 (1), 42–52. <https://doi.org/10.1016/j.jconhyd.2008.07.008>.
- Chaves, M.M., Maroco, J.P., Pereira, J.S., 2003. Understanding plant responses to drought – from genes to the whole plant. *Funct. Plant Biol.* 30 (3), 239–264. <https://doi.org/10.1071/FP02076>.
- Chen, J., Zhu, H., Li, X., 2016. Automatic extraction of discontinuity orientation from rock mass surface 3D point cloud. *Comput. Geosci.* 95, 18–31. <https://doi.org/10.1016/j.cageo.2016.06.015>.
- Chiu, Y., & Chia, Y. (2012). The impact of groundwater discharge to the Hsueh-Shan tunnel on the water resources in Northern Taiwan, (1), 1599–1611. <https://doi.org/10.1007/s10040-012-0895-6>.
- Fan, Y., Miguez-Macho, G., Jobbágy, E.G., Jackson, R.B., Otero-Casal, C., 2017. Hydrologic regulation of plant rooting depth. *Proc. Natl. Acad. Sci.* 114 (40), 10572–10577. Retrieved from <http://www.pnas.org/content/114/40/10572.abstract>.
- Feddes, R.A., 1978. Simulation of field water use and crop yield. *Simulation of Plant Growth and Crop Production*. Pudoc, Wageningen, pp. 194–209.
- Furr, J.R., Reeve, J.O., 1945. Range of soil-moisture percentages through which plants undergo permanent wilting in some soils from semiarid irrigated areas. *J. Agric. Res.* 71 (4), 149–170.
- van Genuchten, M.T., 1980. A closed-form equation for predicting the hydraulic conductivity of unsaturated soils. *Soil Sci. Soc. Am. J.* 44 (5), 892. <https://doi.org/10.2136/sssaj1980.03615995004400050002x>.
- Gisbert, J., Vallejos, A., Gonzalez, A., Pulido-Bosch, A., 2009. Environmental and hydro-geological problems in karstic terrains crossed by tunnels: a case study. *Environ. Geol.* 58 (2), 347–357. <https://doi.org/10.1007/s00254-008-1609-1>.
- Granier, A., Loustau, D., Breda, N., 2000. A generic model of forest canopy conductance dependent on climate, soil water availability and leaf area index. *Ann. For. Sci.* 57 (8), 755–765. <https://doi.org/10.1051/forest:2000158>.
- Hendrickson, A.H., Veihmeyer, F.J., 1945. Permanent wilting percentages of soils obtained from field and laboratory trials. *Plant Physiol.* 20 (4), 517–539.
- Huang, Y., Bao, Y., Wang, Y., 2015. Analysis of geoenvironmental hazards in urban underground space development in Shanghai. *Nat. Hazards* 75 (3), 2067–2079. <https://doi.org/10.1007/s11069-014-1414-y>.
- de Jong van Lier, Q., Metselaar, K., van Dam, J.C., 2006. Root water extraction and limiting soil hydraulic conditions estimated by numerical simulation. *Vadose Zone J.* 6 (3), 527. <https://doi.org/10.2136/vzj2007.0042L>.
- Jukaine, Laine, J., Vasander, H., Laiho, R., 1995. Long-term effects of water level draw-down on the vegetation of drained pine mires in southern Finland. *J. Appl. Ecol.* 32 (4), 785–802. <https://doi.org/10.2307/2404818>.
- Kelln, C.J., Barbour, S.L., Qualizza, C., 2009. Fracture-dominated subsurface flow and transport in a sloping reclamation cover. *Vadose Zone J.* 8, 96–107. <https://doi.org/10.2136/vzj2008.0064>.
- Kim, Y.-Y., Lee, K.-K., 2008. Disturbance of groundwater table by subway construction in the Seoul area, Korea. *Geosci. J.* 7 (1), 37–46. <https://doi.org/10.1007/bf02910263>.
- Kirkham, M.B., 2014. Field capacity, wilting point, available water, and the nonlimiting water range. *Princ. Soil Plant Water Relat.* 153–170. <https://doi.org/10.1016/B978-0-12-420022-7.00010-0>.
- Kong, J., Xin, P., Hua, G.F., Luo, Z.Y., Shen, C.J., Chen, D., Li, L., 2015. Effects of vadose zone on groundwater table fluctuations in unconfined aquifers. *J. Hydrol.* 528, 397–407. <https://doi.org/10.1016/j.jhydrol.2015.06.045>.
- Kvæerner, J., Snilsberg, P., 2008. The romeriksporten railway tunnel – drainage effects on peatlands in the lake Northern Pottjeren area. *Eng. Geol.* 101 (3–4), 75–88. <https://doi.org/10.1016/j.enggeo.2008.04.002>.
- Lenhard, R.J., Parker, J.C., Kaluarachchi, J.J., 1991. Comparing simulated and experimental hysteretic two-phase transient fluid flow phenomena. *Water Resour. Res.* 27 (8), 2113–2124. <https://doi.org/10.1029/91WR01272>.
- Li, L., Tu, W., Shi, S., Chen, J., Zhang, Y., 2016a. Mechanism of water inrush in tunnel construction in Karst area. *Geomat. Nat. Hazards Risk* 7 (sup1), 35–46. <https://doi.org/10.1080/19475705.2016.1181342>.
- Li, X., Chen, J., Zhu, H., 2016b. A new method for automated discontinuity trace mapping on rock mass 3D surface model. *Comput. Geosci.* 89, 118–131. <https://doi.org/10.1016/j.cageo.2015.12.010>.
- Li, X., Li, Y., Chang, C.F., Tan, B., Chen, Z., Sege, J., et al., 2018. Stochastic, goal-oriented rapid modeling of uncertainty and environmental impacts in poorly-sampled sites using ex-situ priors. *Adv. Water Resour.* 111 (November), 174–191. <https://doi.org/10.1016/j.advwatres.2017.11.008>.

- Likos, W.J., Lu, N., Godt, J.W., 2014. Hysteresis and uncertainty in soil water-retention curve parameters. *J. Geotech. Geoenviron. Eng.* 140 (4), 04013050. [https://doi.org/10.1061/\(ASCE\)GT.1943-5606.0001071](https://doi.org/10.1061/(ASCE)GT.1943-5606.0001071).
- Liu, J., Liu, D., Song, K., 2015a. Evaluation of the influence caused by tunnel construction on groundwater environment: a case study of Tongluoshan tunnel, China. *Adv. Mater. Sci. Eng.* 2015. <https://doi.org/10.1155/2015/149265>.
- Liu, X., Li, Y., Chen, X., Zhou, G., Cheng, J., Zhang, D., et al., 2015b. Partitioning evapotranspiration in an intact forested watershed in southern China. *Ecology* 8 (6), 1037–1047. <https://doi.org/10.1002/eco.1561>.
- Miguez-Macho, G., Li, H., Fan, Y., 2008. Simulated water table and soil moisture climatology over North America. *Bull. Am. Meteorol. Soc.* 89 (5), 663–672. <https://doi.org/10.1175/BAMS-89-5-663>.
- Minghe, L., Ritchie, G.A., 1999. Eight hundred years of clonal forestry in China: II. Mass production of rooted cuttings of Chinese fir (*Cunninghamia lanceolata* (Lamb.) Hook). *New For.* 18 (2), 143–159. <https://doi.org/10.1023/A:1006553115255>.
- Monteith, J.L., 1997. Evaporation, evapotranspiration and climatic data: R. Burman and L.O. Pochoy, Elsevier, Amsterdam, The Netherlands, 1994. *J. Hydrol.* 190 (1), 167–168. [https://doi.org/10.1016/S0022-1694\(97\)83310-0](https://doi.org/10.1016/S0022-1694(97)83310-0).
- Mualem, Y., 1976. A new model for predicting the hydraulic conductivity of unsaturated porous media. *Water Resour. Res.* 12 (3), 513–522. <https://doi.org/10.1029/WR012i003p00513>.
- Nielsen, D.R., Luckner, L., 1992. Theoretical aspects to estimate reasonable initial parameters and range limits in identification procedures for soil hydraulic properties. In: *Proceedings of the International Workshop on Indirect Methods for Estimating the Hydraulic Properties of Unsaturated Soils*, pp. 147–160 Retrieved from <https://eurekamag.com/research/020/476/020476101.php>.
- Norero, A.L. (1969). A Formula to Express Evapotranspiration as a Function of Soil Moisture and Evaporative Demands of the Atmosphere.
- Ouyang, S., Xiao, K., Zhao, Z., Xiang, W., Xu, C., Lei, P., et al., 2018. Stand transpiration estimates from recalibrated parameters for the granier equation in a Chinese fir (*Cunninghamia lanceolata*) plantation in Southern China. *Forests* 9 (4), 1–17. <https://doi.org/10.3390/f9040162>.
- Parker, J.C., Lenhard, R.J., 1987. A model for hysteretic constitutive relations governing multiphase flow 1. Saturation-pressure relations. *Water Resour. Res.* 23 (12), 2187–2196.
- Raposo, J.R., Molinero, J., Dafonte, J., 2010. Quantitative evaluation of hydrogeological impact produced by tunnel construction using water balance models. *Eng. Geol.* 116 (3–4), 323–332. <https://doi.org/10.1016/j.enggeo.2010.09.014>.
- Romano, N., Brunone, B., Santini, A., 1998. Flow in layered soils. *Adv. Water Resour.* 17 (96), 315–324.
- Rosenberg, D., McCully, P., Pringle, C., 2000. Global-scale environmental effects of hydrological alterations: introduction. *Bioscience* 50 (9), 1–9 doi:10.1641/0006-3568(2000)050[0746:GSEOHJ]2.0.CO;2.
- Sanchez-Vila, X., Guadagnini, A., Carrera, J., 2006. Representative hydraulic conductivities in saturated groundwater flow. *Rev. Geophys.* 44 (3), 1–46. <https://doi.org/10.1029/2005RG000169>.
- Santos, D., A., M., De Jong Van Lier, Q., Van Dam, J.C., Bezerra, A.H.F., 2017. Benchmarking test of empirical root water uptake models. *Hydrol. Earth Syst. Sci.* 21 (1), 473–493. <https://doi.org/10.5194/hess-21-473-2017>.
- Scheidler, S., Huggenberger, P., Butscher, C., Dresmann, H., 2017. Tools to simulate changes in hydraulic flow systems in complex geologic settings affected by tunnel excavation. *Bull. Eng. Geol. Environ.* <https://doi.org/10.1007/s10064-017-1113-5>.
- Simmer, C., Thiele-Eich, I., Masbou, M., Amelung, W., Bogena, H., Crewell, S., et al., 2014. Monitoring and modeling the terrestrial system from pores to catchments: the transregional collaborative research center on patterns in the soil-vegetation-atmosphere system. *Bull. Am. Meteorol. Soc.* 96 (10), 1765–1787. <https://doi.org/10.1175/BAMS-D-13-00134.1>.
- Šimunek, J., Vogel, T., van Genuchten, M.T., 1992. SWMS-2D Code for Simulating Water Flow and Solute Transport in Two-dimensional Variably Saturated Media: Version 1.1. U.S. Salinity Laboratory Retrieved from <https://books.google.com/books?id=c-RyHQAACA>.
- Šimunek, J., M. Šejna, A., Saito, H., Sakai, M., & Van Genuchten, M.T. (2013). The HYDRUS-1D Software Package for Simulating the Movement of Water, Heat, and Multiple Solutes in Variably Saturated Media, Version 4.17, HYDRUS Software Series 3, (June), 343.
- Slatyer, R.O. (1957). The Significance of the Permanent Wilting Percentage in Studies of Plant and Soil Relations, X(10).
- Sweetenham, M.G., Maxwell, R.M., Santi, P.M., 2017. Assessing the timing and magnitude of precipitation-induced seepage into tunnels bored through fractured rock. *Tunn. Undergr. Space Technol.* 65, 62–75. <https://doi.org/10.1016/j.tust.2017.02.003>.
- Taylor, H.M., Klepper, B., 1979. In: T.-A., N.C.B., Brady, A. (Eds.), *The Role of Rooting Characteristics in the Supply of Water to Plants*, 30. Academic Press, pp. 99–128, Journal Paper J-8906 of the Iowa Agriculture and Home Economics Experiment Station, Ames, Iowa, Project No. 1941, and Technical Paper 4673 of the Oregon State University Agricultural Ex. [https://doi.org/10.1016/S0065-2113\(08\)60704-X](https://doi.org/10.1016/S0065-2113(08)60704-X).
- Tietje, O., Hennings, V., 1996. Accuracy of the saturated hydraulic conductivity prediction by pedo-transfer functions compared to the variability within FAO textural classes. *Geoderma* 69 (1), 71–84. [https://doi.org/10.1016/0016-7061\(95\)00050-X](https://doi.org/10.1016/0016-7061(95)00050-X).
- Vik, E.A., Sverdrup, L., Kelley, A., Storhaug, R., Beitnes, A., Boge, K., et al., 2000. Experiences from environmental risk management of chemical grouting agents used during construction of the Romeriksporten tunnel. *Tunn. Undergr. Space Technol.* 15 (4), 369–378. [https://doi.org/10.1016/S0886-7798\(01\)00006-2](https://doi.org/10.1016/S0886-7798(01)00006-2).
- Vincenzi, V., Gargini, A., Goldscheider, N., 2009. Using tracer tests and hydrological observations to evaluate effects of tunnel drainage on groundwater and surface waters in the Northern Apennines (Italy). *Hydrogeol. J.* 17 (1), 135–150. <https://doi.org/10.1007/s10040-008-0371-5>.
- Vincenzi, V., Gargini, A., Goldscheider, N., Piccinini, L., 2014. Differential hydrogeological effects of draining tunnels through the northern Apennines, Italy. *Rock Mech. Rock Eng.* 47 (3), 947–965. <https://doi.org/10.1007/s00603-013-0378-7>.
- van Walsum, P.E.V., Groenendijk, P., 2008. Quasi steady-state simulation of the unsaturated zone in groundwater modeling of lowland regions. *Vadose Zone J.* 7 (2), 769. <https://doi.org/10.2136/vzj2007.0146>.
- Wang, T.T., Zhan, S.S., Chen, C.H., Su, W.C., 2017. Characterizing fractures to mitigate inrush of water into a shaft using hydrogeological approaches. *Tunn. Undergr. Space Technol.* 61, 205–220. <https://doi.org/10.1016/j.tust.2016.10.011>.
- Yeh, T.-C.J., 1989. One-dimensional steady state infiltration in heterogeneous soils. *Water Resour. Res.* 25 (10), 2149–2158. <https://doi.org/10.1029/WR025i10p2149>.
- Yu, G.R., Zhuang, J., Nakayama, K., Jin, Y., 2007. Root water uptake and profile soil water as affected by vertical root distribution. *Plant Ecol.* 189 (1), 15–30. <https://doi.org/10.1007/s11258-006-9163-y>.
- Yu, L., Zeng, Y., Su, Z., Cai, H., Zheng, Z., 2016. The effect of different evapotranspiration methods on portraying soil water dynamics and et partitioning in a semi-arid environment in Northwest China. *Hydrol. Earth Syst. Sci.* 20 (3), 975–990. <https://doi.org/10.5194/hess-20-975-2016>.
- Zeng, X., Decker, M., 2009. Improving the numerical solution of soil moisture-based Richards equation for land models with a deep or shallow water table. *J. Hydrometeorol.* 10 (1), 308–319. <https://doi.org/10.1175/2008JHM1011.1>.
- Zhang, J.C., DeAngelis, D.L., Zhuang, J.Y., 2011a. A study on plant roots and soil anti-scourability in the Shangshe catchment, Dabie mountains of Anhui Province, China. *Theory and Practice of Soil Loss Control in Eastern China*. Springer Science & Business Media, pp. 243–255.
- Zhang, J.C., DeAngelis, D.L., Zhuang, J.Y., 2011b. Ecological and environmental characteristics in the hilly region of middle and lower Yangtze river bt. In: Zhang, J.C., DeAngelis, D.L., Zhuang, J.Y. (Eds.), *Theory and Practice of Soil Loss Control in Eastern China*. Springer New York, New York, NY, pp. 3–27. https://doi.org/10.1007/978-1-4419-9679-4_1.
- Zhang, Y.K., Schilling, K.E., 2006. Effects of land cover on water table, soil moisture, evapotranspiration, and groundwater recharge: a field observation and analysis. *J. Hydrol.* 319 (1–4), 328–338. <https://doi.org/10.1016/j.jhydrol.2005.06.044>.
- Zhu, Y., Shi, L., Lin, L., Yang, J., Ye, M., 2012. A fully coupled numerical modeling for regional unsaturated-saturated water flow. *J. Hydrol.* 475, 188–203. <https://doi.org/10.1016/j.jhydrol.2012.09.048>.
- Zhuang, J., Yu, G.R., Nakayama, K., 2001. Scaling of root length density of maize in the field profile. *Plant Soil* 235 (1982), 135–142.